**Atmospheric
Measurement
Techniques
Discussions**

Twin Doppler Rayleigh/Mie/Raman lidar for wind and temperature measurements in the middle atmosphere up to 80 km

G. Baumgarten

Leibniz-Institute of Atmospheric Physics at the Rostock University,
18225 Kühlungsborn, Germany

Correspondence to: G. Baumgarten (baumgarten@iap-kborn.de)

AMTD

3, 2779–2803, 2010

Doppler wind and temperature from Rayleigh lidar

G. Baumgarten

Abstract

A direct detection Doppler shift system for measuring wind speed in the middle atmosphere up to 80 km with 2 h resolution was implemented in the ALOMAR Rayleigh/Mie/Raman lidar (69° N, 16° E). The statistical uncertainty of the line of sight wind is about 0.6 m/s and 10 m/s at 49 km and 80 km, respectively. We use a Doppler Rayleigh Iodine Spectrometer (DoRIS) at the iodine line 1109 (∼532.260 nm). DoRIS uses two branches of intensity cascaded channels to cover the dynamic range from 10 to 100 km altitude. The wind detection system was designed to extend the existing multi-color observations of aerosol and temperature. The lidar uses two lasers with a mean power of 14 W at 532 nm each and two 1.8 m diameter tiltable telescopes. Below about 49 km altitude the accuracy and time resolution is limited by the maximum count rate of the detectors used and not by the number of photons available. We report about the first simultaneous Rayleigh temperature and wind measurements by lidar in the strato- and mesosphere on 17 and 23 January 2009.

1 Introduction

Wind measurements are essential for understanding the dynamics in the middle atmosphere on small (<100 km) to global scales. Lidar measurements in the altitude range from 15 km to 70 km are needed (Meriwether and Gerrard, 2004) as there is no other remote sensing method capable to study the time/altitude cross section of temperatures and winds in the so-called radar gap (Fig. 1). Although the basic concepts for lidar wind measurements were introduced and applied about two decades ago, the technical realization is challenging (e.g., Chanin et al., 1989; Rees and McDermid, 1990; Tepley et al., 1991). Several methods for lidar wind measurements to altitudes above 15 km have been proposed and partly demonstrated (e.g., Abreu et al., 1992; Tepley et al., 1993; Liu et al., 1997, 2002). Besides limited experiments demonstrating that the method is feasible, there are up to now only a few reports of regular wind

measurements to about 50 km altitude by Rayleigh lidar (Tepley, 1994; Rees et al., 1996; Friedman et al., 1997; Souprayen et al., 1999).

At the ALOMAR research station in Northern Norway a comprehensive set of instruments is used to study atmospheric dynamics. Meteorological rockets and radiosondes have been used to study the wind profile in a large number of case studies (e.g., Goldberg et al., 2004; Müllemann and Lübken, 2005). Radar observations covering the altitude ranges of 1–15 km (MST radar) and about 60–110 km using the MF radar, SKiYMET meteor radar, or the MST radar are continuously available (Singer et al., 1997, 2003; Latteck, 1999). At the altitude of about 80–105 km measurements with a sodium lidar are performed (Williams et al., 2004). To fill the gap between the radar wind measurements from about 15 km to above 60 km a Doppler Rayleigh wind lidar was developed and installed. Our realization of a Doppler wind lidar is part of a system designed for simultaneous and routine soundings of aerosol, temperature and wind in the middle atmosphere with high stability. Up to now no simultaneous temperature and wind measurements by Rayleigh lidar have been published (Huang et al., 2009). Here we present the first simultaneous temperature and wind measurements by Rayleigh lidar above 50 km.

2 Method and instrumental setup

Wind measurements with the Rayleigh/Mie/Raman lidar at the ALOMAR research station in Northern Norway (69.3° N, 16.0° E) are performed by direct detection of the Doppler shift. The lidar is in routine operation since 1994 and is among others used for long-term monitoring of the middle atmosphere (von Zahn et al., 2000). For example an extensive dataset of observation of noctilucent clouds (NLC) and their particle properties has been accumulated (Fiedler et al., 2009; Baumgarten and Fiedler, 2008). The design and integration of the Doppler wind capability was performed in a way that the time series of observations was not interrupted. We have developed a single photon spectrometer analyzing the Doppler shift of the Cabannes line using iodine

Doppler wind and temperature from Rayleigh lidar

G. Baumgarten

absorption spectroscopy at line 1109 (Young, 1981; She et al., 2007; Gerstenkorn and Luc, 1978). The Cabannes line and the iodine absorption spectrum are shown in Fig. 2. The Doppler shift for 1 m/s wind speed is about 4 MHz or $\Delta\lambda/\lambda \sim 10^{-8}$. The Doppler Rayleigh Iodine Spectrometer (DoRIS) achieves a wavelength precision of $\Delta\lambda/\lambda \sim 10^{-8}$

5 by measuring a signal ratio with a precision of only $S_{I_2}/S_0 \sim 10^{-3}$. Here S_0 and S_{I_2} are the signals before and behind the I_2 cell, respectively. The atmospheric Doppler shift is introduced only by movements along the line of sight. Therefore we use two independently tiltable telescopes (diameter 1.8 m) and two lasers to measure both components of the horizontal wind, projected on the line of sight of the telescopes. The technical

10 realization is depicted in Fig. 3. Light from the two power lasers is guided to the top of the telescopes and emitted coaxially to the optical axis of the receiving telescopes.

The two power lasers are both seeded by one single cw-laser. To achieve a high stability of the seed laser it is in continuous operation and stabilized by iodine absorption spectroscopy to the slope of I_2-line 1109. Over a period of three years the seed laser

15 stability was better than $\Delta\lambda/\lambda = 10^{-8}$ (Fiedler et al., 2008). As the system is designed to measure different atmospheric properties the lasers emit not only 532 nm radiation but also 1064 nm and 355 nm. This reduces the output power at 532 nm (used for DoRIS) and reduces the efficiency of the optics involved. The two power lasers generate a peak power of about 50 MW (14 W average) at 532 nm with a repetition rate

20 of 30 Hz each. Due to imperfections in the seeding process (thermal perturbations etc.) the wavelength of the outgoing laser pulse can show an offset to the seed laser (Nicklaus et al., 2007). Therefore we measure the emitted wavelength during the atmospheric measurements with an I_2 pulse spectrometer (Fiedler et al., 2008). The telescopes are independently tiltable from zenith pointing to 30° off-zenith. One tele-

25 scope (SET) can be tilted to the south-east quadrant, while the other one (NWT) can be tilted to the north-west quadrant. For wind measurements we use either 20° or 30° off-zenith tilt angle, depending on operational requirements e.g. measurements in a common volume with sounding rockets (Baumgarten et al., 2002).

Title Page

Abstract	Introduction
Conclusions	References
Tables	Figures

|◄ | ►|

◄ | ►

Back | Close

Full Screen / Esc

Printer-friendly Version

Interactive Discussion

To simplify the instrumental setup we use only one single polychromatic detection system by coupling the signal of the two telescopes/lasers alternatingly into the detection system. An overview of the detection system is shown in Fig. 4. The time multiplexed analysis of the backscattered light is performed by using a segmented mirror rotating at a frequency of 30 Hz. The detection electronics itself is operated at a repetition frequency of 60 Hz, while the lasers are firing alternatingly with 30 Hz each. Both lasers are synchronized to the chopper in the detection system. After separation of the wavelengths the 532 nm light is guided to the DoRIS spectrometer. We have optimized the spectrometer for stability by choosing an I_2 cell with the most stable absorption spectrum. The I_2 absorption was measured directly by scanning the cw-seed laser. We found that a cell where I_2 is completely in the gas phase (L38 in Fig. 2) gives the best stability. We analyzed the temperature dependence of different cells and found that the spectrometer drift is 36 MHz/K ($\sim$0.03 pm/K) for cells with some I_2 remaining in the bulk phase, due to varying I_2 vapor pressure. For the saturated cells the drift due to Doppler broadening of the I_2-line is only 0.7 MHz/K. This frequency shift corresponds to a wind speed of about 0.18 m/s/K.

The bandwidth of the 532 nm detection branch is 130 pm during nighttime and about 4 pm during day to reduce the solar background. In DoRIS about 60% of the light is sent through the I_2 cell. Due to the absorption in the I_2 this fraction results in about equal signal levels before and behind the cell. The beam diameter at the I_2 cell is 36 mm and we use a cell with a diameter of 50 mm and a length of 150 mm. The temperature is stabilized to better than 0.03 K at about 38 °C. The channel group before the I_2 cell (532 S_0) was used previously for high sensitivity study of NLC throughout the whole day (Fiedler et al., 2005). At the time DoRIS was integrated in the system we changed the detectors from photo multiplier tubes to more efficient avalanche photo diodes to compensate for the signal loss. In total six channels are used for DoRIS, three in front and three behind the cell. The channel groups are intensity cascaded with a splitting ratio of about 50 between high (VH, VDH) and middle (VM, VDM) and middle (VM, VDM) and low (VL, VDL) altitude channels. To monitor the stability of DoRIS, light from

the seeder is sent into the detection system about 1 ms after the start of each single laser pulse. For timing of the seeder light we use the same chopper that defines the timing of the power lasers. After passing the chopper the seeder light is sent through a coupler reproducing the angular intensity distribution from the telescopes and fed into the detection system through BS1 (Fig. 4) which has a reflectivity of higher than 99.99%. The high reflectivity of BS1 was chosen to minimize signal loss from the atmosphere and to attenuate the light from the seeder sufficiently, so it does not overload the high efficiency detectors. Mirrors, dichroics and beam splitters were optimized to have minimal polarization dependence. We repeatedly scanned the cell transmission spectrum using the seed laser in the last three years and could not detect any change. This indicates the stability of the DoRIS spectrometer.

3 Data analysis

The Doppler shift introduced by the movement of air along the line of sight is derived from the signal ratio behind and before the I_2 cell: $D = S_{I_2}/S_0$. This Doppler ratio D is then compared to a modeled set, D_{model}, that was calculated by folding the measured I_2 cell transmission spectrum and the Doppler broadened Cabannes line (Fig. 2). D_{model} was calculated for line of sight wind speeds (w) from -200 m/s to 200 m/s and atmospheric temperatures (T) from 130 K to 340 K. The resulting table of D_{model} is shown (color coded) in Fig. 5a. The seed wavelength was chosen to minimize the dependence of D on temperature to only $\delta D/\delta T = 1.8 \times 10^{-4}$ K^{-1} (Fig. 5b). The wind response is $\delta D/\delta w (w = 0\,\text{m/s}, T = 230\,\text{K}) = 10^{-3}$ m^{-1} s, i.e. 1% per 10 m/s (Fig. 5c). Although the temperature effect on D is small we have to take it into account since the temperatures in the middle atmosphere can range from less than 150 K during summer to more than 320 K during stratospheric warmings (Lübken, 1999; von Zahn et al., 1998). Before calculating wind and temperature the two channel groups "VDH, VDM, VDL" and "VH, VM, VL" are combined to two profiles S_{I_2} and S_0, respectively (Fig. 6). The channels are combined by normalizing the lower altitude channels to VH (or VDH). The temperature

is calculated from S_0 by hydrostatic integration (e.g., Schöch et al., 2008). This retrieval method is valid in the aerosol free part of the atmosphere (usually above 30 km), to calculate wind in the aerosol loaded part of the atmosphere the calculation of D_{model} has to include the aerosol spectral signature. Either temperature measurements using the rotational Raman method ($\lambda=529$ nm and $\lambda=530$ nm in Fig. 4) or from ECMWF (European Center for Medium range Weather Forecast) analysis will give sufficiently precise information to calculate the Doppler broadening of the Cabannes and aerosol line (e.g., Jumelet et al., 2009; Schöch et al., 2008). For the moment we only analyze data in the aerosol free part of the atmosphere. The information about the aerosol load is usually taken from the 1064 nm channel (aerosol and molecular scatter), compared to the 608 nm signal that is generated only from scattering on N_2 molecules.

In the analysis of winds there are two system parameters that are changing with time but need to be known precisely. One is the wavelength offset ($\Delta\lambda_0$) between the power lasers and the seed laser. The other is the signal ratio (D_0) of the two channel groups S_{I_2} and S_0 at the seed wavelength due to varying quantum efficiency of the detectors. Both parameters are measured during operation. From calibration measurements we know that D_0 also depends on the way that the light is feed into the detection system. During calibration we measure D_0 for all entrances (both telescopes and the seeder entrance) simultaneously. During operation we only measure D_0 for the seeder entrance (D_{seeder}) but take the ratio between the seeder entrance and the telescope entrances into account when deriving Doppler winds. We found for the north-west telescope $D_{NWT}=0.9917{\cdot}D_{seeder}$ and for the south-east telescope $D_{SET}=0.8776{\cdot}D_{seeder}$. This system parameter depends on the alignment of the system and basically describes the overlap of the different entrances imaged at the detector and the detector area. The parameter remains constant unless the alignment of the detection system is changed.

4 Initial observations

We have performed a number of DoRIS wind and calibration measurements during January 2009 and we show data from two days (17 and 23 January) analyzed so far. During these two observations the mean wavelength offsets of the power lasers to the seed laser ($\Delta\lambda_0$) were -12.9 MHz and -11.5 MHz for laser 1 and -13.7 MHz and -14.3 MHz for laser 2. On both days we have integrated the profiles for two hours, centered around 18:00 UT. At 18:00 UT data from the ECMWF is available and can be used for comparison to the actual measurements. We use ECMWF analysis data extracted on pressure levels from ground to about 62 km altitude. To investigate the aerosol free altitude range we show the aerosol load in Fig. 7. The aerosol load is described by the backscatter ratio $R=(\beta_a+\beta_m)/\beta_m$. Here β_a and β_m are the backscatter coefficients for aerosols and molecules, respectively. One can see that the top of the aerosol layer varies by more than 10 km within a few days. This is due to the high latitude of the ALOMAR research station where the stratospheric aerosol layer is affected by the polar vortex dynamics (e.g., McCormick et al., 1983; Kent et al., 1985). From the aerosol profiles we realize that on 17 January ALOMAR was located outside the polar vortex, while on 23 January ALOMAR was sounding under the vortex. On 17 January 2009 the NWT was pointing north, 30°off-zenith and the SET was pointing to zenith. Laser 1 was assigned to the NWT and laser 2 to the SET. This pointing was chosen for joint observations with a sounding rocket launched from the Andøya Rocket range during the Delta 2 campaign (e.g., Williams et al., 2006).

In Fig. 6 we show the backscatter profiles (background subtracted) accumulated during two hours of measurements, centered at 18:00 UT on 17 January 2009. The data was acquired with the vertical pointing south-east telescope and laser 2. We have smoothed the data with a 2 km running mean filter. The Doppler ratio calculated from the combination of the channel groups is varying only slightly with altitude. This indicates that the vertical wind is small and not changing systematically with altitude. The variations of the Doppler ratio with altitude are mainly induced by changes in the

Title Page

Abstract | Introduction

Conclusions | References

Tables | Figures

◄ | ►|

◄ | ►

Back | Close

Full Screen / Esc

Printer-friendly Version

Interactive Discussion

atmospheric temperature. This becomes more clear when comparing the Doppler ratio with the temperature deduced from hydrostatic integration. The retrieved temperature and wind components are shown in Fig. 8. The temperature profile is calculated by averaging the measurements of both telescopes. We find the maximum temperature of about 275 K at an altitude of 58 km. At the same altitude the Doppler ratio in Fig. 6 reaches its maximum. During the measurement the atmosphere was disturbed by a developing major stratospheric warming occurring on 24 January 2009 (Labitzke and Kunze, 2009; Manney et al., 2009). We observe a strong wave disturbance in the temperature profile from about 55 to 75 km. From about 58 km to 70 km we observe a quasi adiabatic lapse rate similar to the thermal structure under summer conditions. The stratospheric warming can be seen in the disturbed temperature profile and especially in the unusual meridional wind profile. Under typical winter conditions the meridional wind is much lower and shows no upper stratospheric southward directed jet. We pointed one telescope to zenith to investigate the quality of the system as the 2 h average vertical winds should be below our detection threshold. The vertical wind profile in Fig. 8 shows that the vertical wind profile is constant with altitude and shows no extreme values at 58 km altitude, where we observed the highest temperatures. The resulting nearly zero vertical wind, although the measured channel ratio was not constant with altitude, demonstrates that the temperature effect (Doppler broadening) is correctly treated in the wind retrieval. The meridional wind in Fig. 8 agrees with the ECMWF analysis taking the coarser altitude resolution of the model into account.

In Fig. 8 we also show results from the SKiYMET meteor radar averaged from 17:00 to 19:00 UT. We find that at the top of the altitude range covered by the lidar the meridional wind agrees well with the wind derived from the collocated radar instrument. The statistical uncertainty of the line of sight wind is 9 m/s and 19 m/s for the horizontal wind at 80 km. The gray area in Fig. 8 indicates aerosol loaded altitudes where more than 1% of the signal of the 532 nm channel or 10% of the signal of the 1064 nm channel are scattered from aerosol particles. Retrieved winds in these altitudes could be biased as we do not take aerosol contributions into account yet.

On 23 January 2009 the NWT and SET were pointing 20° off-zenith to north and east, respectively. Figure 9 shows temperature and both components of the horizontal wind measured from 17:00 to 19:00 UT. We again observe a good agreement of the structure with the ECMWF wind and excellent agreement of lidar and radar winds at the top of the lidar profile. It should be noted that large temperature offsets of ECMWF temperatures and observed temperatures similar to the 10…30 K differences shown in Figs. 8 and 9 have been reported earlier (Schöch et al., 2008). At altitudes above 30 km deviations of about 25 K have been observed for observations on scales of a few hours. These large differences occur especially during stratospheric warmings. At the same time the mean deviations on monthly scales are about 3 K and less. As there is no systematic investigation of wind observations and ECMWF winds at around the stratopause available yet, we find our agreement between lidar and ECMWF already noteworthy and remaining differences will be investigated in future. We observe remarkable changes in the thermal and dynamical structure of the atmosphere as the stratospheric warming evolves. This is partly caused by the location of the polar vortex which changed from 17 to 23 January.

From the ECMWF data in Fig. 10 one can see that ALOMAR is sounding low latitude air masses with high ozone values on 17 January, while there were polar air masses above ALOMAR with low ozone at 25 km on 23 January. This is in excellent agreement with the aerosol observations that indicated that ALOMAR is outside the vortex on 17 January but inside on 23 January. On 23 January the vortex is almost split which can be seen in Fig. 10. The figure shows that ECMWF horizontal wind speeds are larger than 120 m/s and up to 200 m/s in the upper stratosphere. The DoRIS wind precision of better than 20 m/s up to 80 km is well suited to measure such wind speeds, especially at the stratopause where the precision for lidar wind soundings is about 1…3 m/s. Under daylight conditions the top altitude for temperature soundings decreases by about 20 km. At the same time the MF radar wind observations reach lower down under sunlight conditions, hence the combination of lidar and radar winds will allow for continuous wind soundings throughout the strato- and mesosphere.

5 Conclusions

The ALOMAR RMR lidar was successfully enhanced to perform Doppler wind measurements throughout the strato- and mesosphere without interrupting the long-term observation of temperature and aerosols in the middle atmosphere. The lidar can perform temperature and horizontal wind measurements between about 30 km and 80 km. Using the simultaneously measured aerosol contribution we expect to extend the measurement range. The minimum measurement uncertainty for 2 km range resolution and 2 h time resolution is 0.6 m/s at about 49 km altitude. At an altitude of 80 km the measurement uncertainty increases to about 20 m/s. The fidelity of DoRIS was proven by vertical wind measurements and comparison to independent radar wind measurements. For future analysis we will include aerosol effects especially to deduce wind in noctilucent clouds (∼83 km) which provide a strong signal. This new method for wind measurements improves previous lidar Rayleigh Doppler wind measurements at ALOMAR that did not reach above 30 km on regular basis (Baumgarten et al., 1999). Under favorable conditions the comparison to other wind measurements performed at the ALOMAR research station will be possible. For example the MF radar can provide wind informations down to ∼70 km. Data combination with the sodium resonance lidar at ALOMAR might be possible with the benefit that both instruments use the same sounding volume.

References

Abreu, V. J., Barnes, J. E., and Hays, P. B.: Observations of winds with an incoherent lidar detector, Appl. Optics, 31, 4509–4514, 1992. 2780

Baumgarten, G. and Fiedler, J.: Vertical structure of particle properties and water content in noctilucent clouds, Geophys. Res. Lett., 35, L10811, doi:10.1029/2007GL033084, 2008. 2781

Baumgarten, G., Rees, D., and Lloyd, N. D.: Observations of Arctic Stratospheric Winds by the ALOMAR Doppler Wind and Temperature System, ESA Special Publication, 437, 331–334, 1999. 2789

Baumgarten, G., Lübken, F.-J., and Fricke, K. H.: First observation of one noctilucent cloud by a twin lidar in two different directions, Ann. Geophys., 20, 1863–1868, doi:10.5194/angeo-20-1863-2002, 2002. 2782

Chanin, M. L., Garnier, A., Hauchecorne, A., and Porteneuve, J.: A Doppler lidar for measuring winds in the middle atmosphere, Geophys. Res. Lett., 16, 1273–1276, doi:10.1029/GL016i011p01273, 1989. 2780

Fiedler, J., Baumgarten, G., and von Cossart, G.: Mean diurnal variations of noctilucent clouds during 7 years of lidar observations at ALOMAR, Ann. Geophys., 23, 1175–1181, doi:10.5194/angeo-23-1175-2005, 2005. 2783

Fiedler, J., Baumgarten, G., and von Cossart, G.: A middle atmosphere lidar for multi-parameter measurements at a remote site, in: Papers presented at the 24th ILRC, 824–827, 2008. 2782

Fiedler, J., Baumgarten, G., and Lübken, F.-J.: NLC observations during one solar cycle above ALOMAR, J. Atmos. Sol.-Terr. Phy., 71, 424–433, doi:10.1016/j.jastp.2008.11.010, 2009. 2781

Friedman, J. S., Tepley, C. A., Castleberg, P. A., and Roe, H.: Middle-atmospheric Dopplerlidar using an iodine-vapor edge filter, Opt. Lett., 22, 1648–1650, doi:10.1364/OL.22.001648, 1997. 2781

Gerstenkorn, S. and Luc, P.: Atlas du spectre d'absorption de la molecule d'iode, in: Edition du CNRS, Paris, 1978. 2782

Goldberg, R. A., Fritts, D. C., Williams, B. P., Lübken, F., Rapp, M., Singer, W., Latteck, R., Hoffmann, P., Müllemann, A., Baumgarten, G., Schmidlin, F. J., She, C., and Krueger, D. A.: The MaCWAVE/MIDAS rocket and ground-based measurements of polar summer dynamics: overview and mean state structure, Geophys. Res. Lett., 31, L24S02,

Doppler wind and temperature from Rayleigh lidar

G. Baumgarten

Title Page

Abstract | Introduction

Conclusions | References

Tables | Figures

◀ | ▶

◀ | ▶

Back | Close

Full Screen / Esc

Printer-friendly Version

Interactive Discussion

doi:10.1029/2004GL019411, 2004. 2781

Huang, W., Chu, X., Williams, B. P., Harrell, S. D., Wiig, J., and She, C.-Y.: Na double-edge magneto-optic filter for Na lidar profiling of wind and temperature in the lower atmosphere, Opt. Lett., 34, 199–201, doi:10.1364/OL.34.000199, 2009. 2781

Jumelet, J., Bekki, S., David, C., Keckhut, P., and Baumgarten, G.: Size distribution time series of a polar stratospheric cloud observed above Arctic Lidar Observatory for Middle Atmosphere Research (ALOMAR) (69° N) and analyzed from multiwavelength lidar measurements during winter 2005, J. Geophys. Res., 114, D02202, doi:10.1029/2008JD010119, 2009. 2785

Kent, G. S., Farrukh, U. O., Trepte, C. R., and McCormick, M. P.: Variation in the stratospheric aerosol associated with the North Cyclonic Polar Vortex as measured by the SAM II satellite sensor, J. Atmos. Sci., 42, 1536–1551, doi:10.1175/1520–0469(1985)042<1536:VITSAA>2.0.CO;2, 1985. 2786

Labitzke, K. and Kunze, M.: On the remarkable Arctic winter in 2008/2009, J. Geophys. Res., 114, D00I02, doi:10.1029/2009JD012273, 2009. 2787

Latteck, R., Singer, W., and Bardey, H.: The ALWIN MST Radar: Technical Design and Performance, in: European Rocket and Balloon Programs and Related Research, edited by: Kaldeich-Schürmann, B., vol. 437 of ESA Special Publication, 1999.

Liu, Z., Wu, D., Liu, J., Zhang, K., Chen, W., Song, X., Hair, J. W., and She, C.: Low-altitude atmospheric wind measurement from the combined Mie and Rayleigh backscattering by Doppler lidar with an iodine filter, Appl. Optics, 41, 7079–7086, doi:10.1364/AO.41.007079, 2002. 2780

Liu, Z. S., Chen, W. B., Zhang, T. L., Hair, J. W., and She, C. Y.: An incoherent Doppler lidar for ground-based atmospheric wind profiling, Appl. Phys. B, 64, 561–566, doi:10.1007/s003400050215, 1997. 2780

Lübken, F.-J.: Thermal structure of the Arctic summer mesosphere, J. Geophys. Res., 104, 9135–9149, doi:10.1029/1999JD900076, 1999. 2784

Manney, G. L., Schwartz, M. J., Krüger, K., Santee, M. L., Pawson, S., Lee, J. N., Daffer, W. H., Fuller, R. A., and Livesey, N. J.: Aura Microwave Limb Sounder observations of dynamics and transport during the record-breaking 2009 Arctic stratospheric major warming, Geophys. Res. Lett., 36, L12815, doi:10.1029/2009GL038586, 2009. 2787

McCormick, M. P., Trepte, C. R., and Kent, G. S.: Spatial changes in the stratospheric aerosol associated with the north polar vortex, Geophys. Res. Lett., 10, 941–944,

Doppler wind and temperature from Rayleigh lidar

G. Baumgarten

doi:10.1029/GL010i010p00941, 1983. 2786

Meriwether, J. W. and Gerrard, A. J.: Mesosphere inversion layers and stratosphere temperature enhancements, Rev. Geophys., 42, RG3003, doi:10.1029/2003RG000133, 2004. 2780

Müllemann, A. and Lübken, F.: Horizontal winds in the mesosphere at high latitudes, Adv. Space Res., 35, 1890–1894, doi:10.1016/j.asr.2004.11.014, 2005. 2781

Nicklaus, K., Morasch, V., Höfer, M., Luttmann, J., Vierkoetter, M., Ostermeyer, M., Höffner, J., Lemmerz, C., and Hoffmann, D.: Frequency stabilization of Q-switched Nd:YAG oscillators for airborne and spaceborne LIDAR systems, in: Proceedings of SPIE, vol. 6451, doi:10.1117/12.701187, 2007. 2782

Rees, D. and McDermid, I. S.: Doppler lidar atmospheric wind sensor – reevaluation of a 355-nm incoherent Doppler lidar, Appl. Optics, 29, 4133–4144, 1990. 2780

Rees, D., Vyssogorets, M., Meredith, N. P., Griffin, E., and Chaxell, Y.: The doppler wind and temperature system of the ALOMAR lidar facility: overview and initial results, J. Atmos. Sol.-Terr. Phy., 58, 1827–1842, 1996. 2781

Schöch, A., Baumgarten, G., and Fiedler, J.: Polar middle atmosphere temperature climatology from Rayleigh lidar measurements at ALOMAR (69° N), Ann. Geophys., 26, 1681–1698, doi:10.5194/angeo-26-1681-2008, 2008. 2785, 2788

She, C.-Y., Yue, J., Yan, Z.-A., Hair, J. W., Guo, J.-J., Wu, S.-H., and Liu, Z.-S.: Direct-detection Doppler wind measurements with a Cabannes Mie lidar: a Comparison between iodine vapor filter and Fabry Perot interferometer methods, Appl. Optics, 46, 4434–4443, doi:10.1364/AO.46.004434, 2007. 2782

Singer, W., Keuer, D., and Eriksen, W.: The ALOMAR MF radar: technical design and first results, in: Proceedings of the 13th ESA Symposium on European Rocket and Balloon Programmes and Related Research, Öland, Sweden, edited by: Kaldeich-Schürmann, B., 101–103, ESA Publications Division, 1997.

Singer, W., Bremer, J., Hocking, W. K., Weiss, J., Latteck, R., and Zecha, M.: Temperature and wind tides around the summer mesopause at middle and Arctic latitudes, Adv. Space Res., 31, 2055–2060, doi:10.1016/S0273–1177(03)00228-X, 2003.

Souprayen, C., Garnier, A., Hertzog, A., Hauchecorne, A., and Porteneuve, J.: Rayleigh-Mie Doppler wind lidar for atmospheric measurements. I. instrumental setup, validation, and first climatological results, Appl. Optics, 38, 2410–2421, doi:10.1364/AO.38.002410, 1999. 2781

Tepley, C. A.: Neutral winds of the middle atmosphere observed at Arecibo using a Doppler Rayleigh lidar, J. Geophys. Res., 99, 25781–25790, doi:10.1029/94JD02213, 1994. 2781

Doppler wind and temperature from Rayleigh lidar

G. Baumgarten

Title Page

Abstract	Introduction
Conclusions	References
Tables	Figures

Back | Close

Full Screen / Esc

Printer-friendly Version

Interactive Discussion

Tepley, C. A., Sargoichev, S. I., and Hines, C. O.: Initial Doppler Rayleigh lidar results from Arecibo, Geophys. Res. Lett., 18, 167–170, doi:10.1029/90GL02670, 1991. 2780

Tepley, C. A., Sargoytchev, S. I., and Rojas, R.: The Doppler Rayleigh lidar system at Arecibo, IEEE T. Geosci. Remote, 31, 36–47, doi:10.1109/36.210442, 1993. 2780

5   von Zahn, U., Fiedler, J., Naujokat, B., Langematz, U., and Krüger, K.: A note on record-high temperatures at the northern polar stratopause in winter 1997/98, Geophys. Res. Lett., 25, 4169–4172, doi:10.1029/1998GL900091, 1998. 2784

von Zahn, U., von Cossart, G., Fiedler, J., Fricke, K. H., Nelke, G., Baumgarten, G., Rees, D., Hauchecorne, A., and Adolfsen, K.: The ALOMAR Rayleigh/Mie/Raman lidar: objectives,

10   configuration, and performance, Ann. Geophys., 18, 815–833, doi:10.1007/s00585-000-0815-2, 2000. 2781

Williams, B. P., Fritts, D. C., Wang, L., She, C. Y., Vance, J. D., Schmidlin, F. J., Goldberg, R. A., Müllemann, A., and Lübken, F.: Gravity waves in the Arctic mesosphere during the MaCWAVE/MIDAS summer rocket program, Geophys. Res. Lett., 31, L24S05,

15   doi:10.1029/2004GL020049, 2004. 2781

Williams, B. P., Fritts, D. C., Vance, J. D., She, C., Abe, T., and Thrane, E.: Sodium lidar measurements of waves and instabilities near the mesopause during the DELTA rocket campaign, Earth Planets Space, 58, 1131–1137, 2006. 2786

Young, A. T.: Rayleigh scattering, Appl. Optics, 20, 533–535, 1981. 2782

Title Page

Abstract | Introduction

Conclusions | References

Tables | Figures

◄ | ►

◄ | ►

Back | Close

Full Screen / Esc

Printer-friendly Version

Interactive Discussion
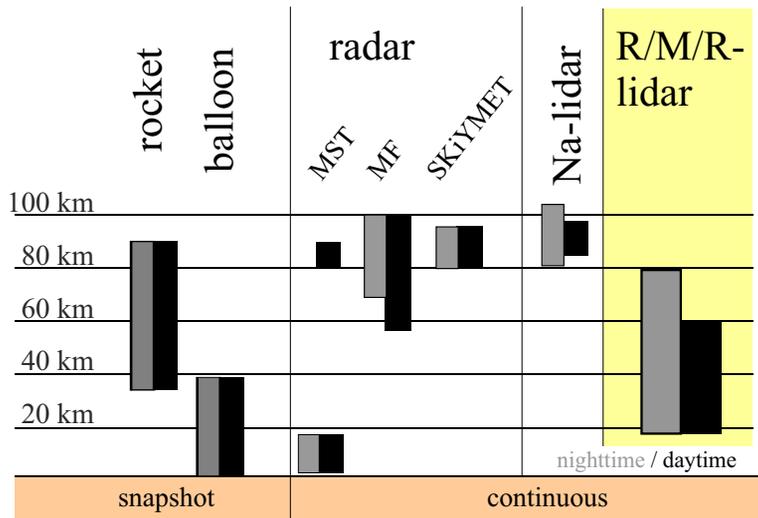
Fig. 1. Altitude range of different methods for sounding wind at the ALOMAR research station in Northern Norway.
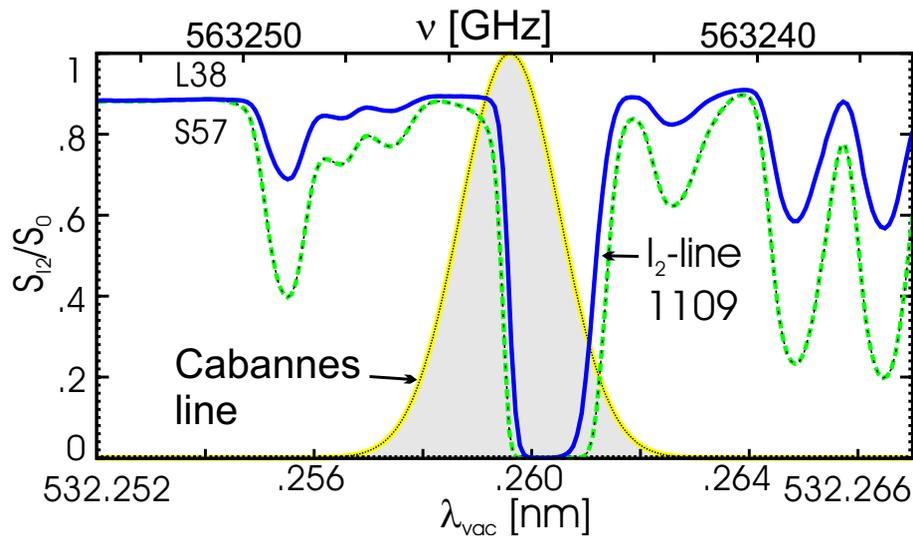
Fig. 2. Measured transmission spectrum of iodine for two cells of different length at different temperatures: 38 °C (blue L38: 15 cm long), 57 °C (green S57: 10 cm long). For reference, the Doppler broadened Cabannes line for 230 K is shown.
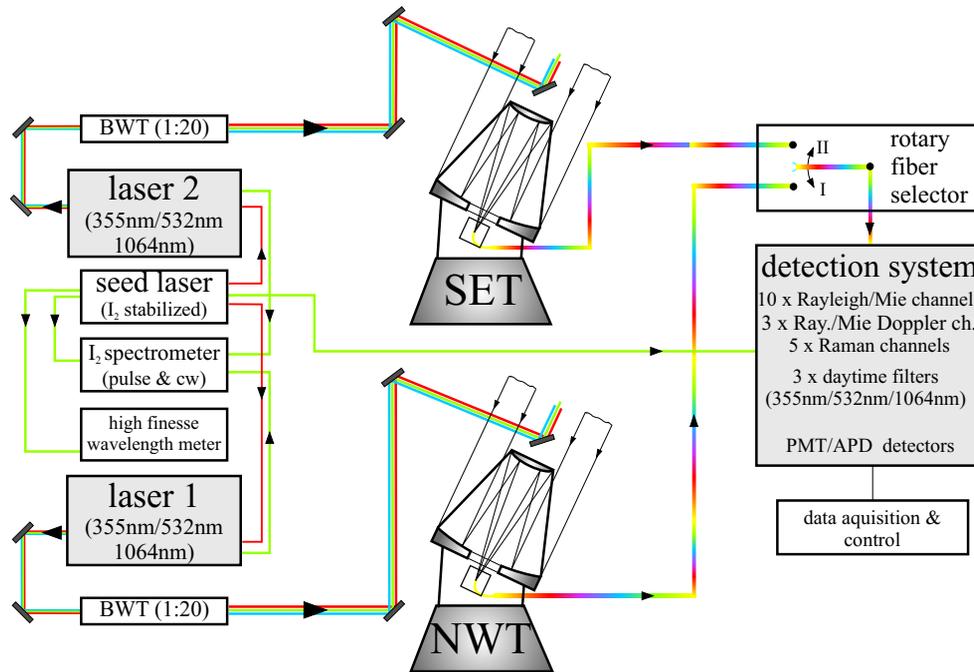
Fig. 3. Overview of the ALOMAR RMR lidar. Two pulsed power lasers (laser 1,2) are seeded with infrared light ($\lambda\sim$1064 nm) by one cw-laser stabilized to iodine absorption line 1109 ($\lambda\sim$532 nm). The optical connection between different components is indicated by red, green, and blue lines to indicate the wavelength of the light, 1064 nm, 532 nm, 355 nm, respectively. The outgoing laser pulses are expanded to a diameter of d=20 cm and guided to the optical axis of two tiltable telescopes (d=1.8 m). The light collected by the telescopes is guided through fibers (d=1.5 mm) to the detection system.

Title Page

Abstract | Introduction

Conclusions | References

Tables | Figures

◄ | ►

◄ | ►

Back | Close

Full Screen / Esc

Printer-friendly Version

Interactive Discussion
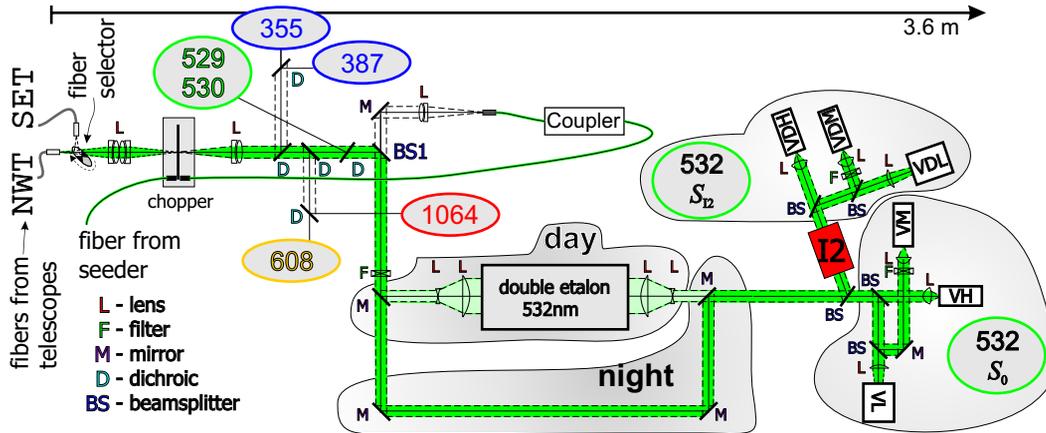
Fig. 4. Polychromatic detection system of the ALOMAR RMR lidar with emphasis on 532 nm channels. Light from the telescopes (NWT or SET) is split by wavelength and intensity. Light for the DoRIS system is detected by the channel groups 532-S_0 and 532-S_{I_2}. The system can be operated during day using a double etalon system (bandpass ~4 pm).
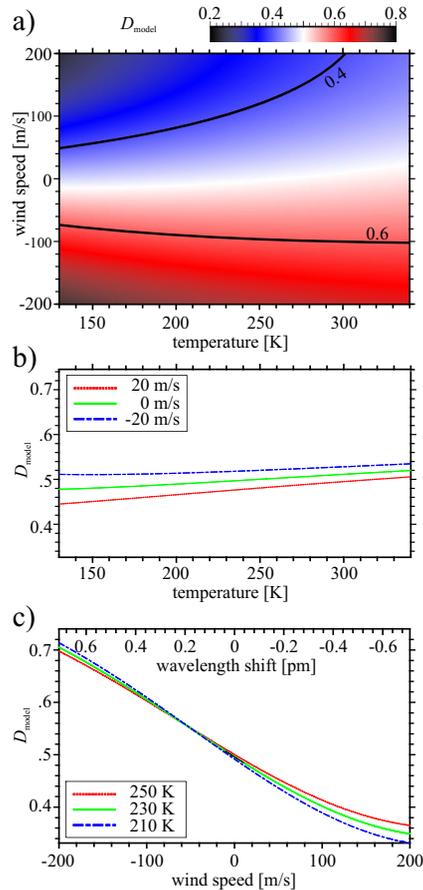
Fig. 5. Modeled Doppler ratio D_{model} for different combinations of temperature and wind speed. **(a)** Color coded atmospheric temperature and wind response. **(b)** Temperature response for 0, +20, −20 m/s wind speed. **(c)** Wind response for atmospheric temperatures of 210, 230, 250 K.
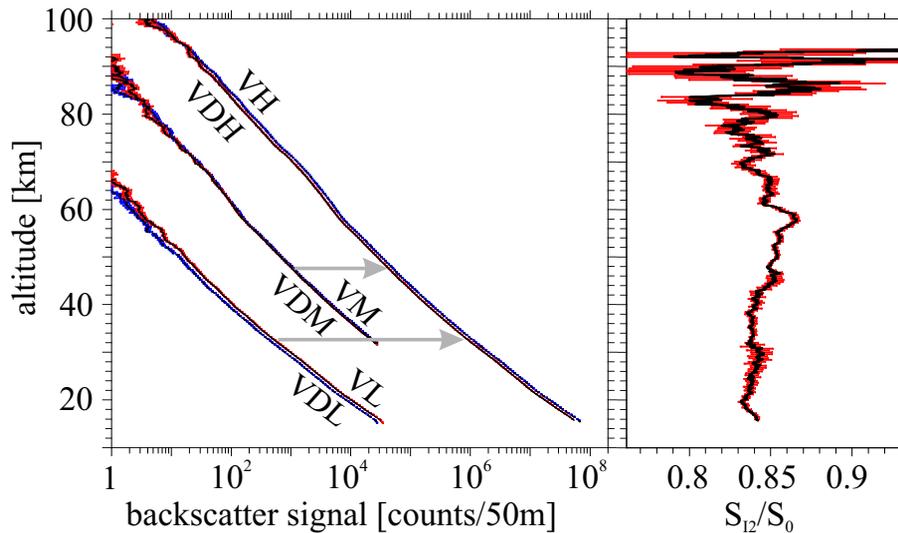
Fig. 6. Left: Backscatter profile of the vertical pointing telescope on 17 January 2009 from 17:00 to 19:00 UT. Data of the channel groups "VDH, VDM, VDL" (black/blue) and "VH, VM, VL" (black/red) is combined to two profiles S_{I_2} and S_0, respectively. Right: Measured Doppler ratio $D=S_{I_2}/S_0$. The measurement uncertainty (1σ) is indicated by red or blue horizontal bars.
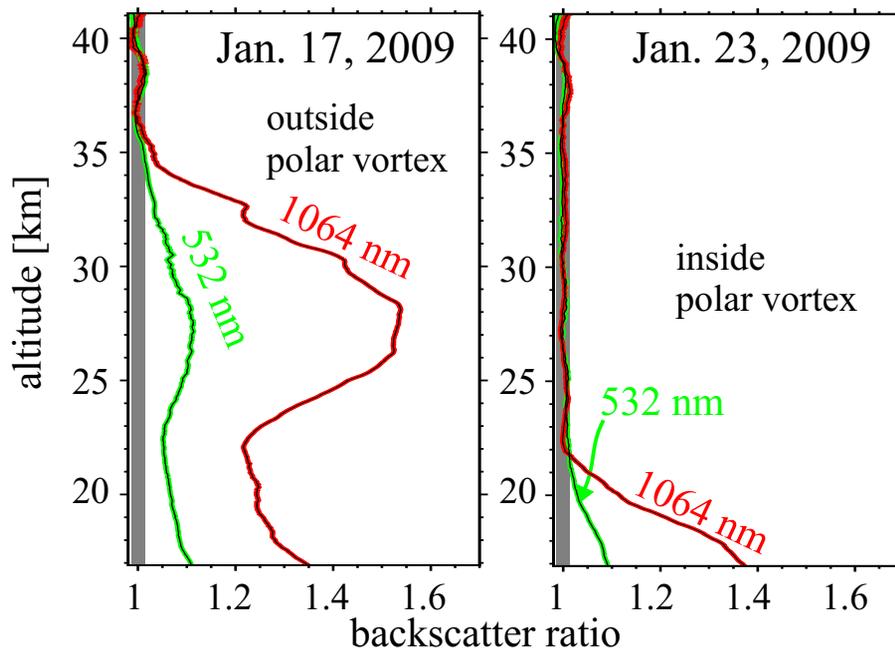
Fig. 7. Aerosol backscatter ratio during the measurements on 17 and 23 January 2009. The gray vertical bar indicates the aerosol free signal ±1%. The measurement uncertainty is indicated by the thickness of the green and red lines. The aerosol contribution to the signal was less than 1% at 532 nm for altitudes above 34 km and 22 km on 17 and 23 January, respectively. The data is smoothed using a running mean of about 2 km.

Title Page

Abstract | Introduction

Conclusions | References

Tables | Figures

◀ | ▶

◀ | ▶

Back | Close

Full Screen / Esc

Printer-friendly Version

Interactive Discussion
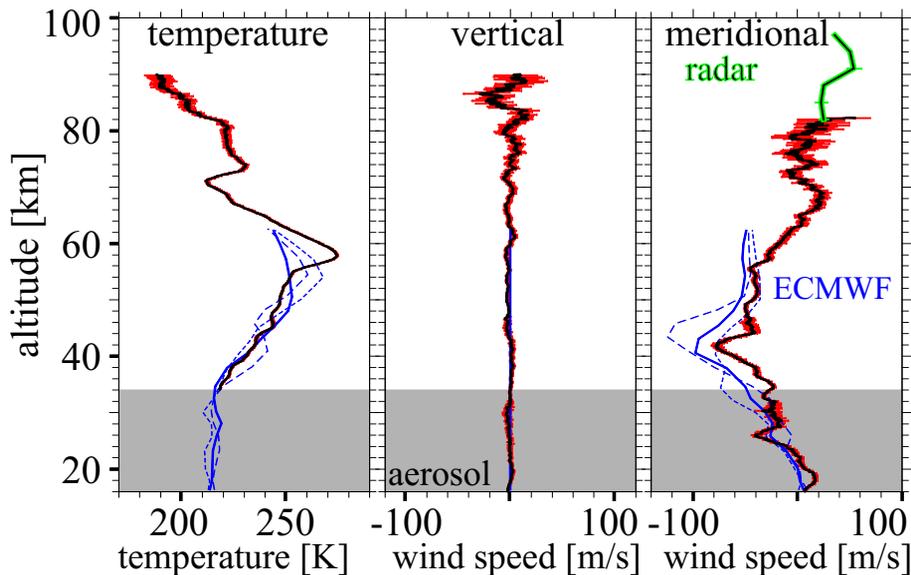
Fig. 8. Temperature, vertical and meridional wind on 17 January 2009 between 17:00 and 19:00 UT. ECMWF data from 18:00 UT (solid) and 12:00, 24:00 UT (dashed) are shown. Simultaneous observations by the collocated Meteor radar are shown. The gray area indicates altitudes with aerosol contribution as measured by the lidar.
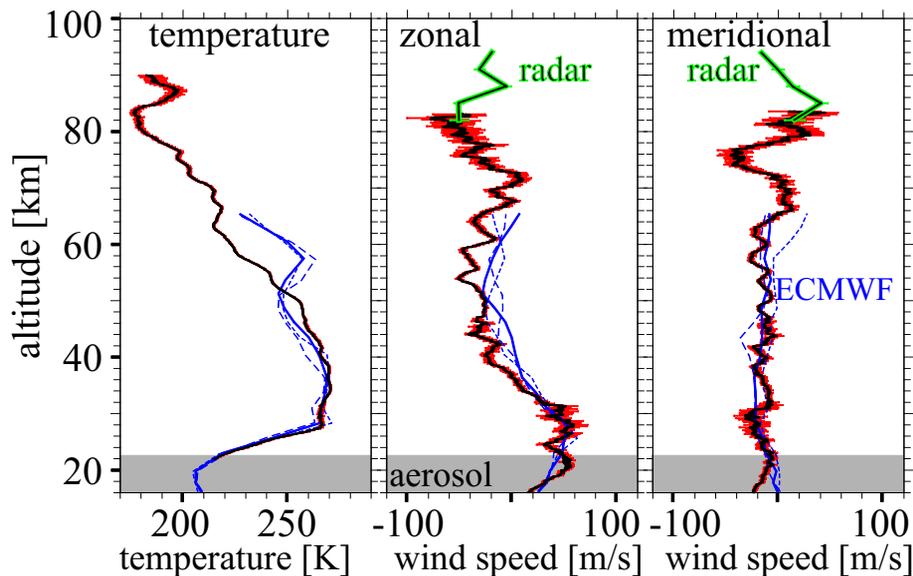
Fig. 9. Temperature and horizontal wind on 23 January 2009 between 17:00 and 19:00 UT. More details in Fig. 8.

Title Page

Abstract | Introduction

Conclusions | References

Tables | Figures

|◄ | ►|

◄ | ►

Back | Close

Full Screen / Esc

Printer-friendly Version

Interactive Discussion

January 17, 2009   January 23, 2009
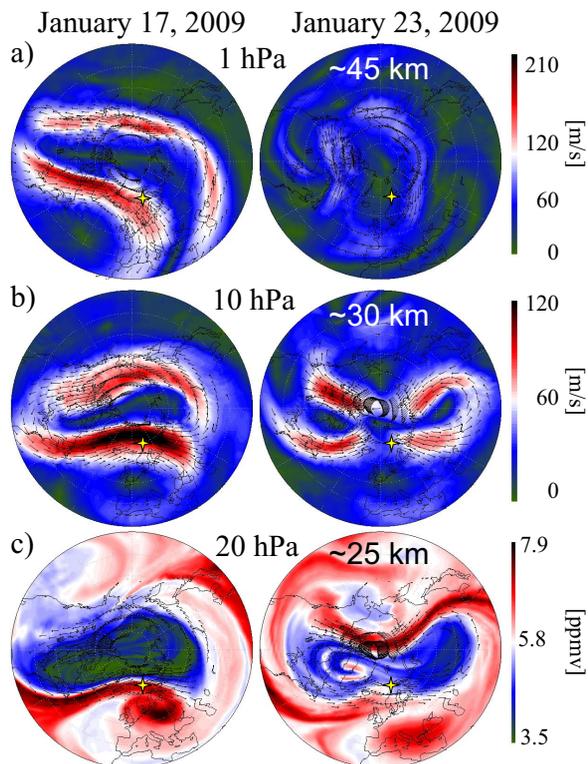
Fig. 10. Horizontal wind and ozone concentration on different levels on 17 January and 23 January 2009 18:00 UT extracted from ECMWF (European Center for Medium range Weather Forecast) operational analysis. **(a)** Horizontal wind at 1 hPa level (∼45 km). **(b)** Horizontal wind at 10 hPa level (∼30 km). **(c)** Ozone (color contour) and horizontal wind (vectors) at 20 hPa level (∼25 km). Wind vectors are only plotted for wind speeds larger than 40 m/s. Please note that the color scale is changing for the different pressure levels. The location of ALOMAR is indicated by a yellow star. Greenwich Meridian is found at the bottom of the plots.

Title Page

Abstract   Introduction

Conclusions   References

Tables   Figures

◄   ►

◄   ►

Back   Close

Full Screen / Esc

Printer-friendly Version

Interactive Discussion